Modeling of radio frequency heating and current drive in tokamaks in the ion cyclotron and lower hybrid frequency ranges.

Massively parallel programming, integrated multiscale, multiphysics modelling.

John Wright - PSFC@MIT

October 10, 2013 - CHATS 10^{th} Applied Superconductivity workshop, Cambridge, MA

Participants in the Center for Simulation of Wave-Plasma Interactions

P.T. Bonoli, J.C. Wright, A. Ram

D. L. Green, D.B. Batchelor, L. A. Berry,
E.F. Jaeger, E. D`Azevedo

C.K. Phillips, E. Valeo
N. Bertelli

R.W. Harvey, Y. Petrov
A.P. Smirnov, J. Kinsey

CompX

D. Smithe

D. D'Ippolito, J. Myra

M. Choi
IMSOL-X

M. Brambilla
R. Bilato

R. Maggiora
Politecnico di Torino

Contents

Motivation

Self-consistency: Radio frequency waves in plasmas are an important tool for profile control via heating and current drive to maintain the magnetic equilibrium.

- Ion cyclotron (IC) waves - affect ion distribution: minority tail
- Lower hybrid (LH) waves - affect electron distribution: quasilinear plateau

Radio frequency waves in magnetically confined plasmas may modify the particle distribution functions which in turn affects the wave dielectric.
Validation: Synthetic diagnostics are a technique in which computational results are mapped to experimental measurements as a basic for comparison and validation.

- Phase contrast imaging (PCI) and Compact Neutral Particle Analyzer (CNPA) for IC
- Hard X-Ray diagnostic (HXR) for LH

Numerical challenges results from physics at different time scales

- Maxwell's equations in the frequency domain, ω:
  $$\boldsymbol{\nabla}\times\boldsymbol{\nabla}\times\mathbf{E} = \frac{\omega^2}{c^2}\left\{\mathbf{E} + \frac{4\pi i}{\omega}\left(\mathbf{J}^P + \mathbf{J}^A\right)\right\}$$
  $$\mathbf{E} = \sum_{m,n} \mathbf{E}_{m,n}(r)\exp\left(im\theta + in\phi\right) \text{ or } \mathbf{E} = \sum_{n,m,l} \mathbf{E}_{n,m,l}\exp\left(i(k_n R + k_m Z + l\phi)\right)$$

- The plasma current, $\mathbf{J}^P = \int \overleftrightarrow{\sigma}(x,x')\cdot\mathbf{E}(x')$, is an integral operator that may be evaluated analytically in a spectral basis [Stix, 1992] or by numerically following orbits along characteristics.
- The dielectric response, $\overleftrightarrow{\sigma}(x,x') \propto \int \hat{H}_u f_0(u) d^3u$ is determined by the distribution function, $f_0(u)$, which in turn is evolved on a longer timescale (than $1/\omega$) by the Fokker-Planck equation:
  $$\partial(\lambda f_0)/\partial t = C(f_0) + D_{\mathrm{ql}}(E^2, f_0).$$
  or Monte Carlo approach or direct calculation of Newtonian response.
- Solving this nonlinear, coupled set of PDEs requires an iterative process to attain self-consistency.

Waves Regimes

Simplified view of ICRF physics

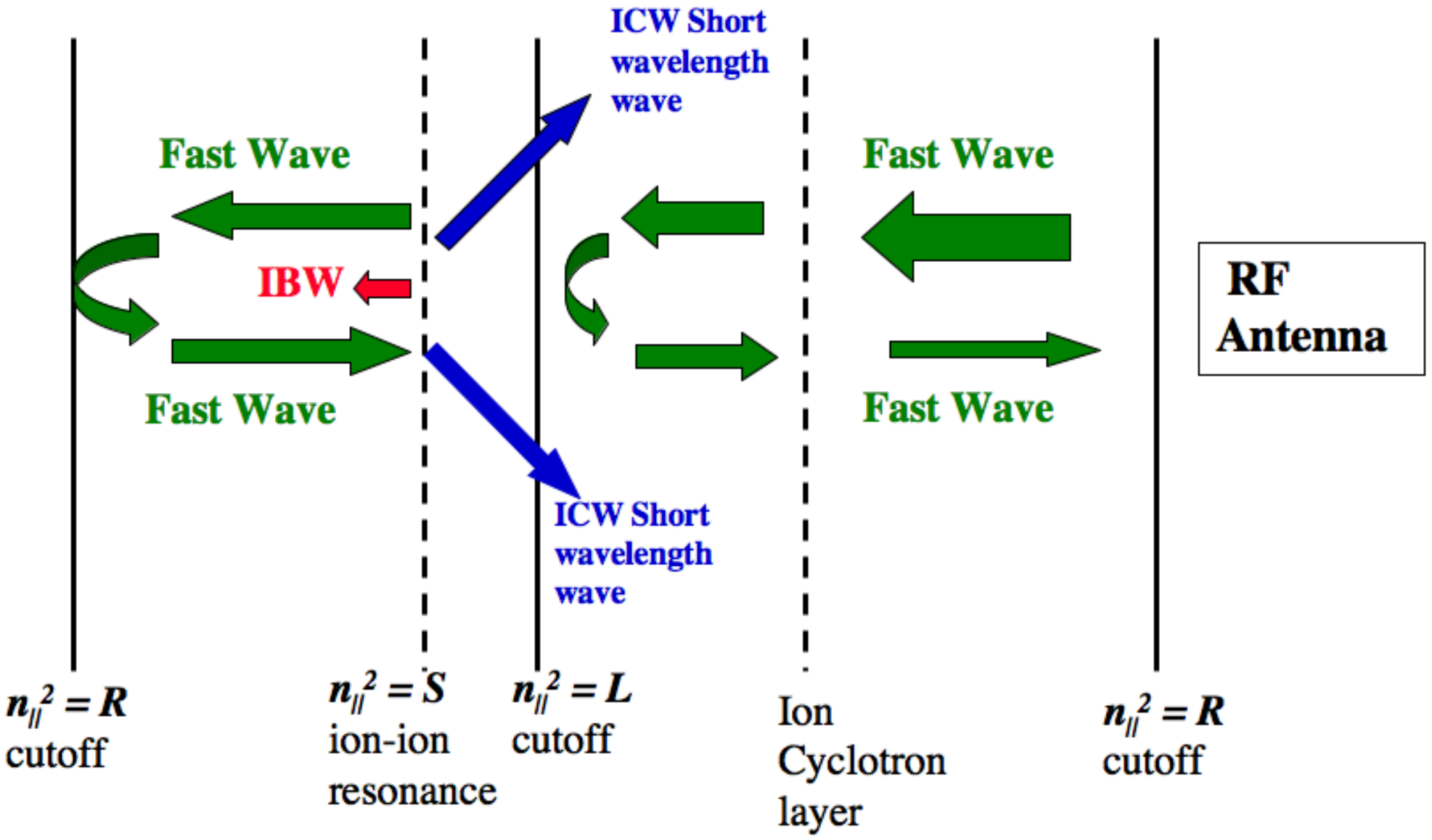

[Courtesy of Y. Lin]

Mode conversion from FW to ICW and IBW

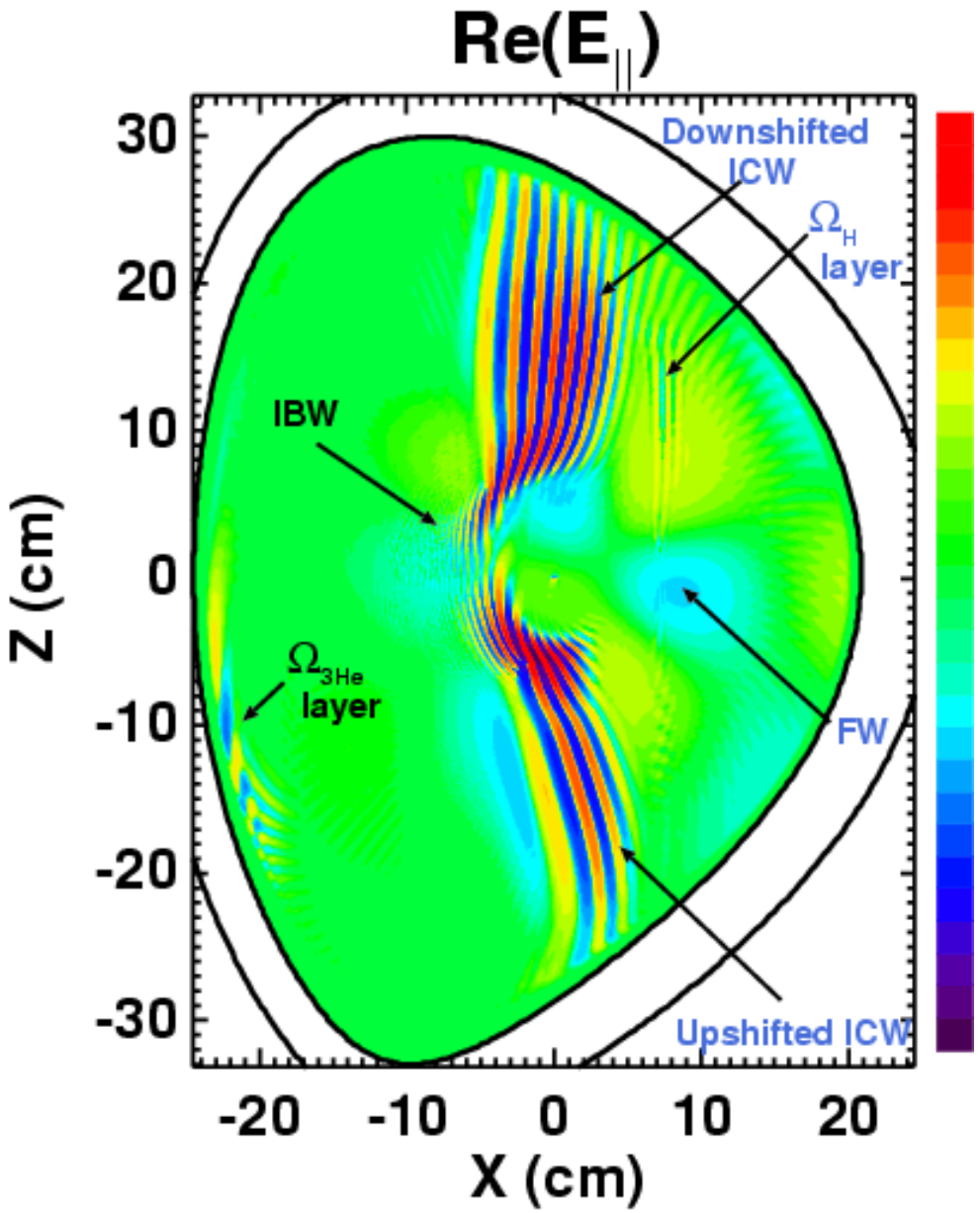

- Simulations of mode conversion are easily achieved with parallelization.(Typically N_m=255xNr=480)
- All three waves branches are apparent.
- ICW: a key example of simulation led discovery in experiments

  [Nelson-Melby *et al.*, 2003, Jaeger *et al.*, 2003] . From 'strange IBW' to 'flow drive' tool.

IBW is on axis, ICW is off axis

- IBW : electrostatic waves propagate along the midplane.
- ICW : these wave require a poloidal field and are coupled off the midplane [Perkins, 1977] .
- FW : the launched wave, appears as the large scale fluctuation. Some transmits through and reflects from the high field side cutoff.

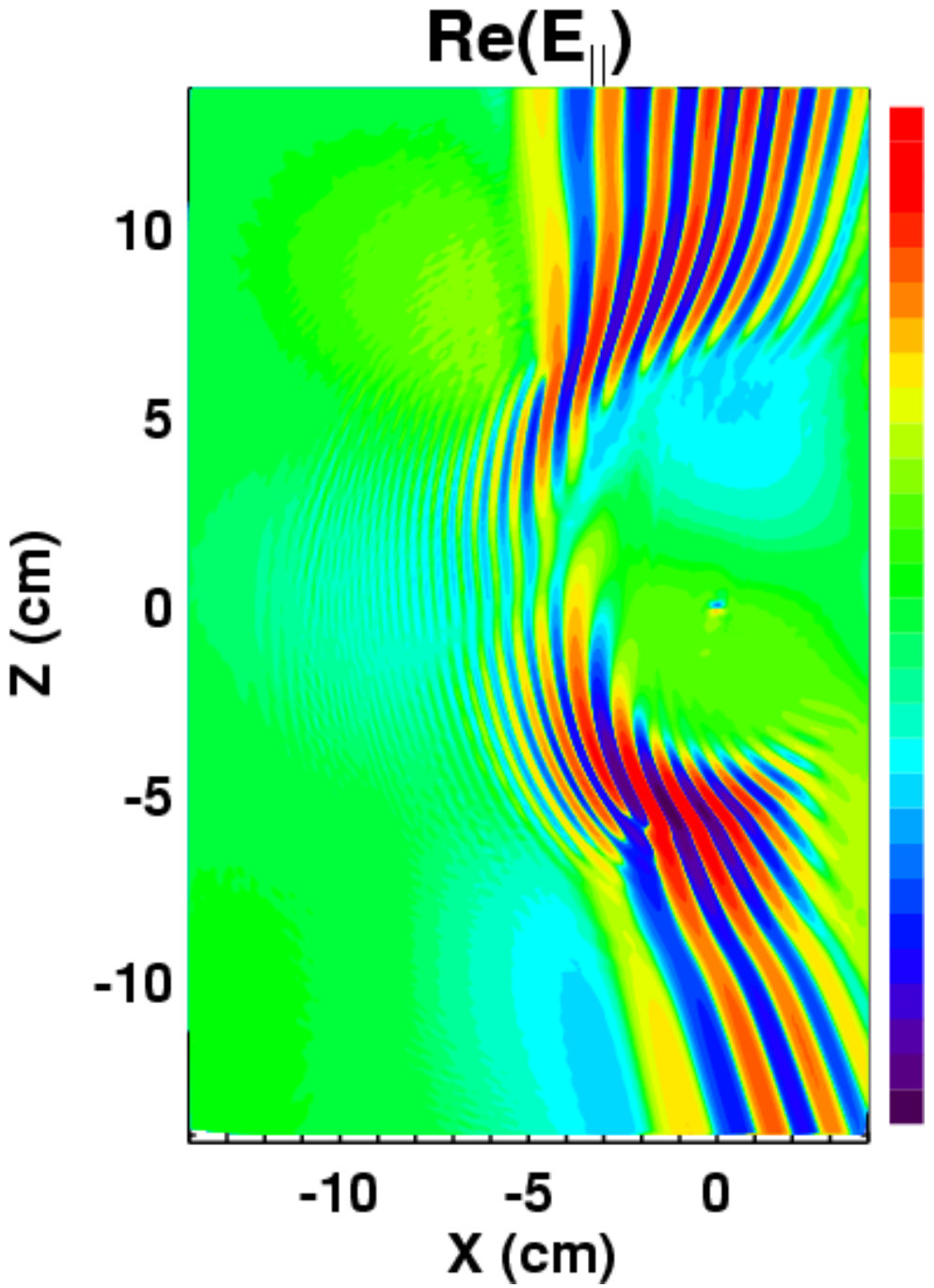

Lower Hybrid wave introduction

- Frequency range: $\omega \sim \sqrt{\Omega_{\rm ce}\Omega_{\rm ci}} \sim 4.7$ GHz
- Unmagnetized ions
- Strongly magnetized electrons
- Two propagating modes: fast and **slow** wave, $\omega/k_{\parallel} \gg v_{\rm te}$

- Wavelengths are very short
  $\lambda_{\perp} \approx \frac{\omega}{\omega_{\rm pe}}\lambda_{\parallel} \approx 1$mm
  $\rightarrow N_{\rm m} \approx 1000 - 2000.$
- For efficient electron current drive, operate at
  $\omega > 2\omega_{\rm LH}$
- Predicts an accessibility criterion:
  $n_{\parallel} >= n_{\parallel {\rm a}} \equiv \frac{\omega_{\rm pe}}{\Omega_{\rm ce}} + \sqrt{S}$

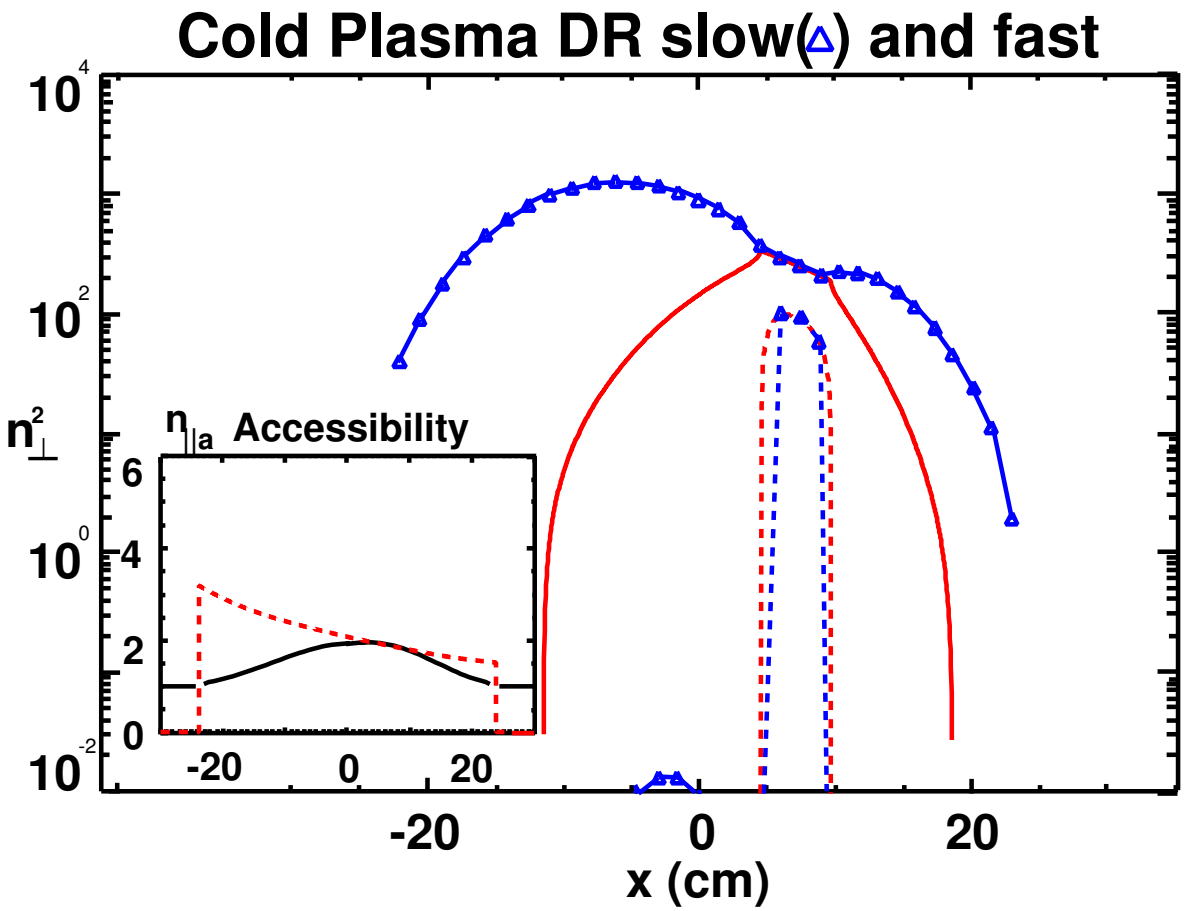

LH Absorption physics

- Parallel refractive indexes are geometrically up-shifted as waves propagate to smaller major radius. Poloidal asymmetries can cause spread in poloidal spectrum.

$$n_{\|} = \frac{c}{\omega}(m/q + n)/R$$

- Quasilinear damping occurs at $\omega/(k_{\|} v_{\mathrm{te}}) \sim 3$:

$$n_{\|} \approx \frac{5.7}{\sqrt{T_e[\mathrm{keV}]}},$$

  so lower temperatures require higher $n_{\|}$ for damping.
- Higher parallel refractive indexes are more accessible to the interior of the plasma but also damp at lower temperatures=larger minor radii.
- Current drive scales as $1/n_{e0} n_{\|}^2$ and $n_{\mathrm{acc}}[n_{e0}, B]$ sets minimum $n_{\|}$ => operation in weak damping regime for $T_{e0} < 16\mathrm{keV}$

Iteration for self-consistency needed in LHRF

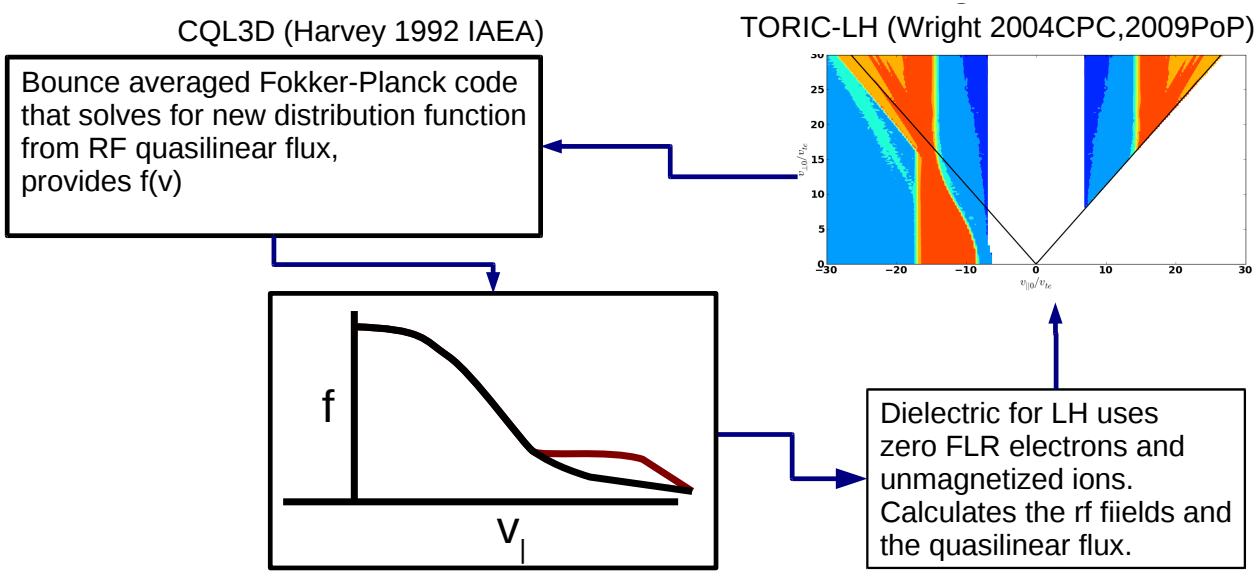

- A fixed point (Picard) iteration scheme is used:

$$Dql_{n+1} = WE(f_n)$$
$$f_{n+1} = FP(f_n, Dql_n)$$

- This technique is known to converge slowly in many instances.
- It can also be unstable in cases of weak ($n_{\|}^2 < 40/T_e$) absorption.

Numerical Techniques to the rescue

TORIC's Large Matrix solved directly

$$\underset{\Rightarrow}{\mathbf{A}} \cdot \mathbf{E} = \mathbf{J}_A \text{ where } \underset{\Rightarrow}{\mathbf{A}} = \begin{pmatrix} \mathbf{D}_1 & \mathbf{U}_1 & \mathbf{0} & \mathbf{0} & \mathbf{0} \\ \mathbf{L}_2 & \mathbf{D}_2 & \mathbf{U}_2 & \mathbf{0} & \mathbf{0} \\ \mathbf{0} & \ddots & \ddots & \ddots & \mathbf{0} \\ \mathbf{0} & \mathbf{0} & \mathbf{L}_{Nm-1} & \mathbf{D}_{Nm-1} & \mathbf{U}_{Nm-1} \\ \mathbf{0} & \mathbf{0} & \mathbf{0} & \mathbf{L}_{Nm} & \mathbf{D}_{Nm} \end{pmatrix}$$

- Discretizing the wave eqn produces a matrix equation. The blocks, **L**, **D**, and **U** are each dense matrices of size $\mathcal{O}(6N_m)^2$.
- The individual $3N_r$ blocks are distributed across the processors and inverted using `(SCA)LaPack` to do an **LU** decomposition.
- Processor memory limitations on simulation sizes are removed by using an out-of-core technique in which block inverses are stored on local disks. Performance saturates as nprocs $\approx (N_m/\text{blocksize})^2$

Multiple contexts used to increase parallelism.

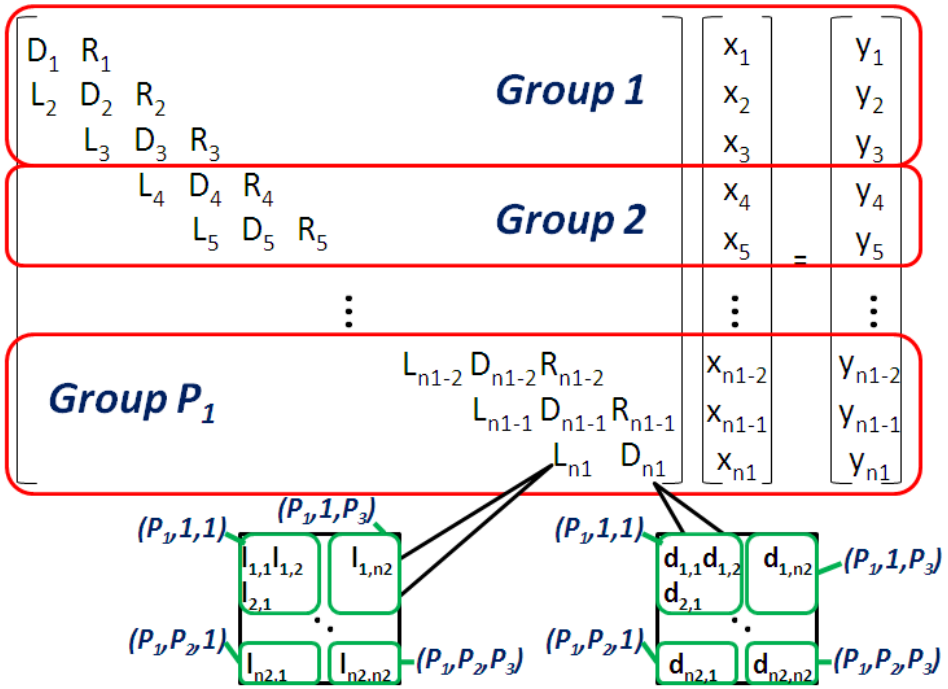

- A schematic of the 3-dimensional parallelization for a block-tridiagonal system. The size of each block, L, D and R is n2 n2 ,and there are n1 rows of the blocks. The rows are divided by P1 groups, and the element of each block is assigned to P2P3 processors. So, every element has a 3-dimensional index of the assigned processor among total number of processors, Ptot =P1P2P3.
- Block rows are distributed among several parallel contexts to form a 3D processor grid for solving the block tri-diagonal system.
- A combination of block-cyclic and divide and conquer is used [Garaud and Garaud, 2008, Lee and Wright, 2013]
- Floating point work is increased but communication intensity is decreased improving overall strong scaling.

Scaling of new solver

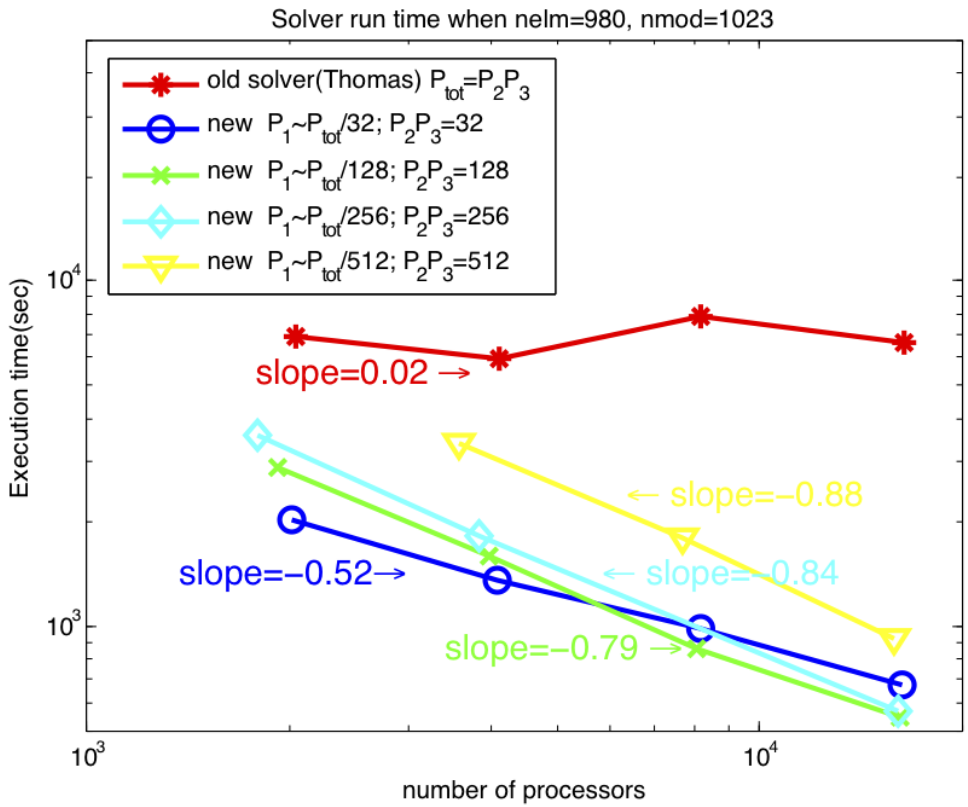

- Old solver is saturated already at 1024 processors
- New solver continues to scale past 10 000 processors
- Speed up is due in part to reduced communication but also improved floating point rate from reduced integer ops (bigger loops) and probably improved pipelining.

Python is used for loose coupling

- 3-D reconstruction python driven with batch jobs dispatched for each toroidal mode. Separate script for reconstruction and export in VTK format for visualization by VisIT.
- Python script for handling automation of `CQL3D-TORLH` /`AORSA` iteration.
- XML source generation of fortran namelist files with auto unit transformation
  1. Runs `CQL3D` [Harvey and McCoy, 1993] and `TORLH` [Wright *et al.*, 2010] or `AORSA` [Jaeger *et al.*, 2002] in batch jobs with locking to enforce run order
  2. Copies files, makes directories and links for next iteration
  3. Ensures input consistency across multiple input files for physics and numerical parameters.

Some applications

Iteration with Fokker-Planck

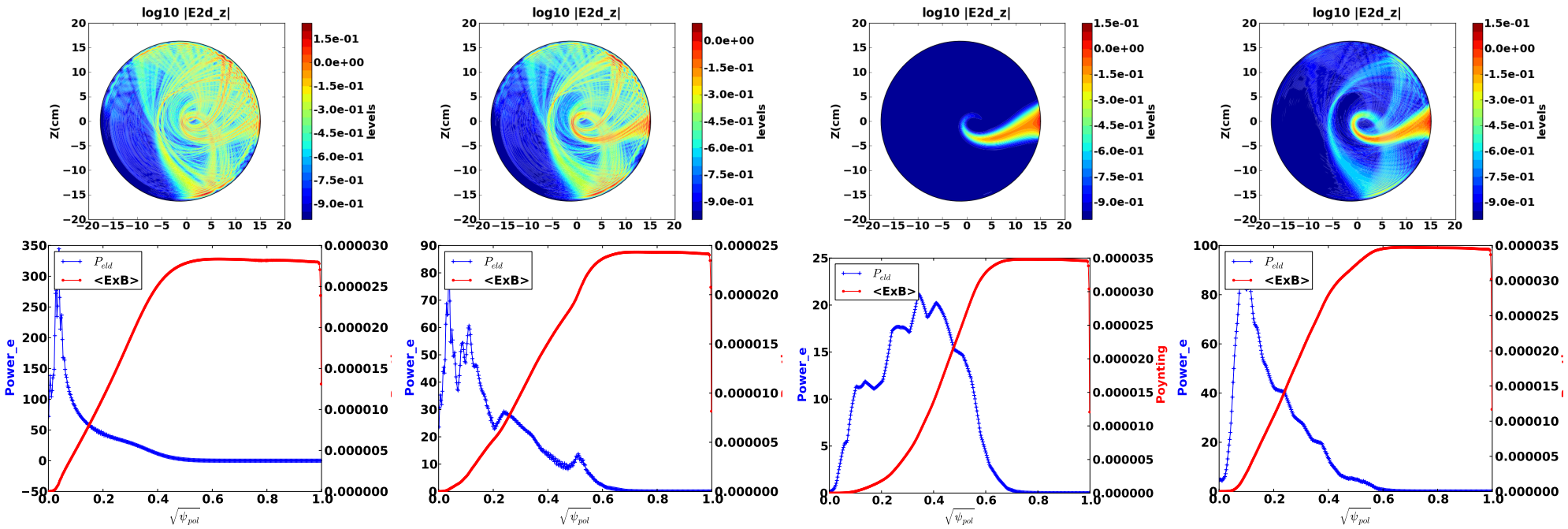

Iteration #

- Converges after some oscillations in damping strength.
- Power of 350 kW generates 150 kA. ($n_{\|} = -2.5$, $T_e = 2.5keV$)
- Resolution, `TORLH` [Wright *et al.*, 2010] $400N_r \times 255N_m$,
  `CQL3D` [Harvey and McCoy, 1993] $60N_r \times 88N_\mu \times 160N_u$

Converged at Step 5.

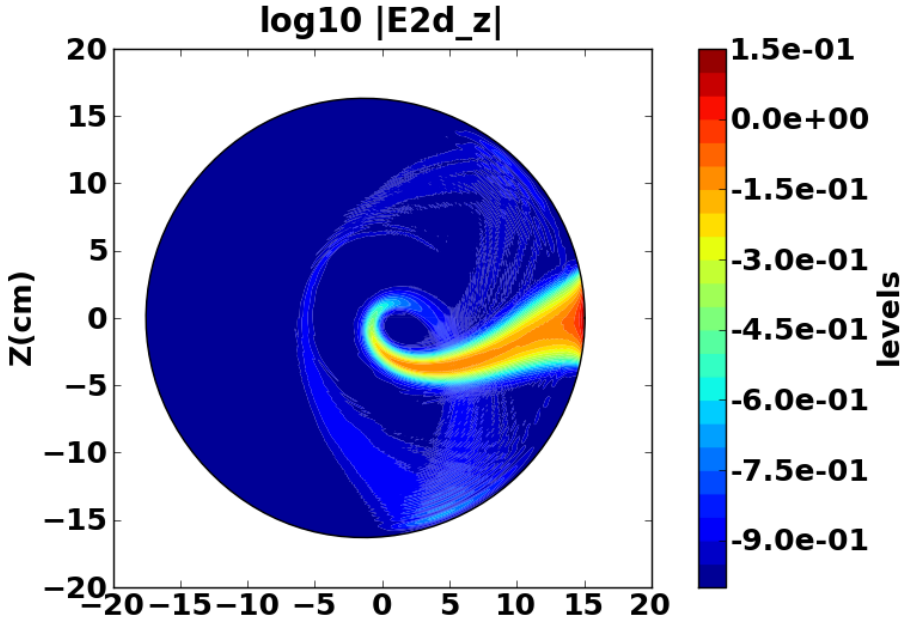

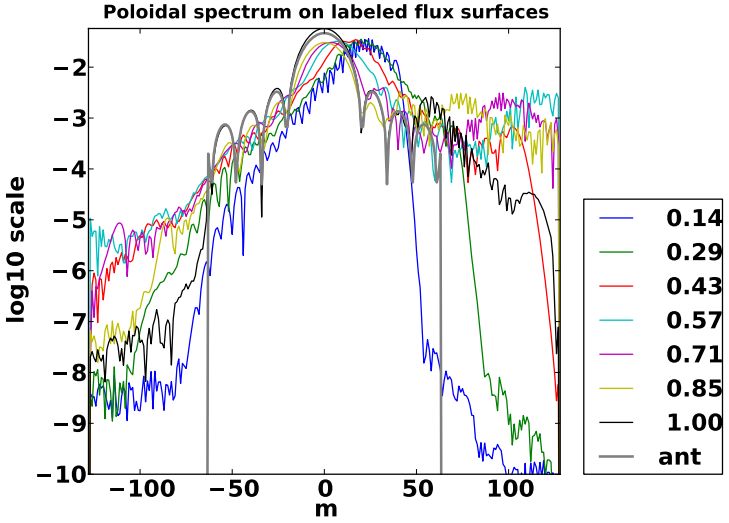

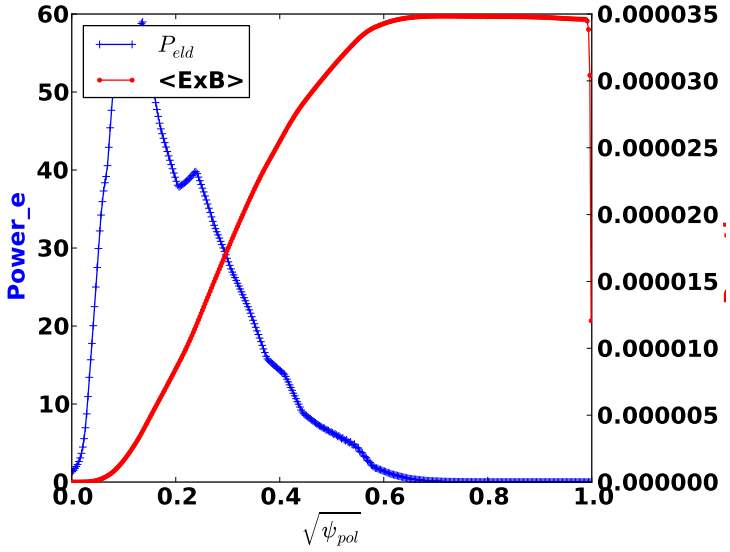

Three dimensional simulations show resonant cone structure in fields.

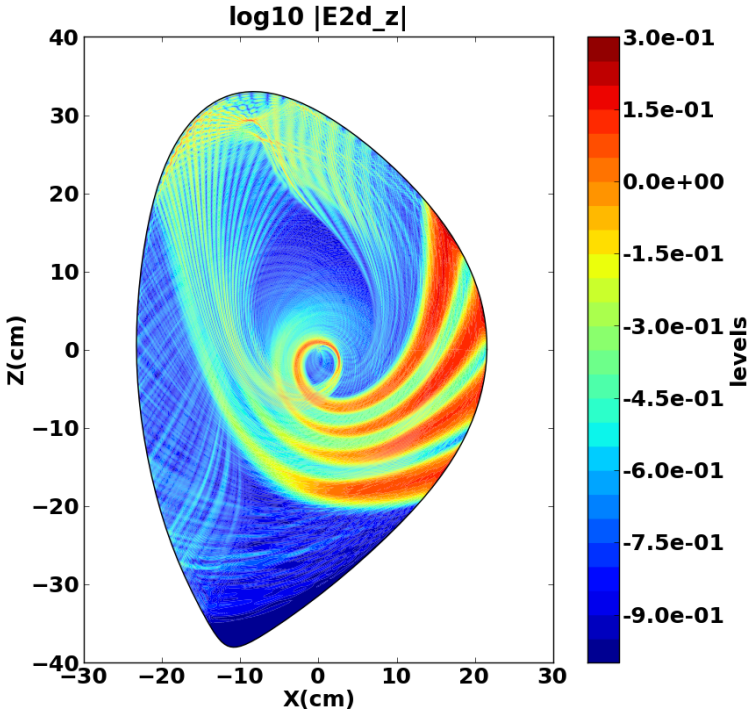

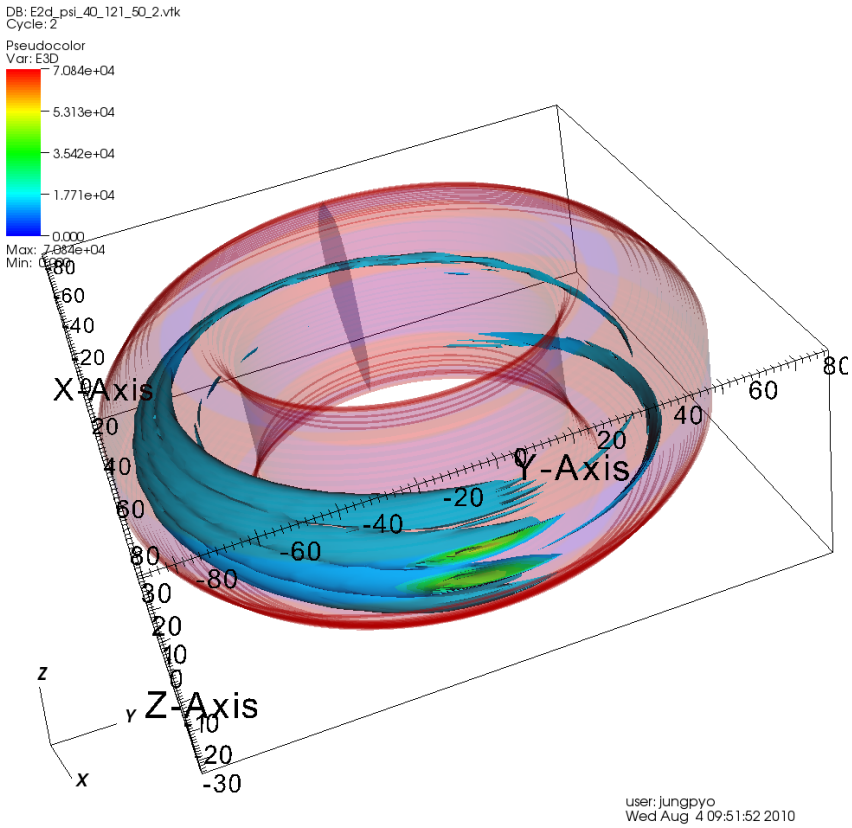

- Converged field patterns shown at 8th iteration between `TORLH` and `CQL3D` in Alcator C-Mod ($n_{\|} = -1.9$).
- 3-D fields obtained by superposing results from 20 toroidal modes.
- 3-D fields exhibit characteristic resonance cone behavior.

C-Mod $n_{\|} = -1.55$

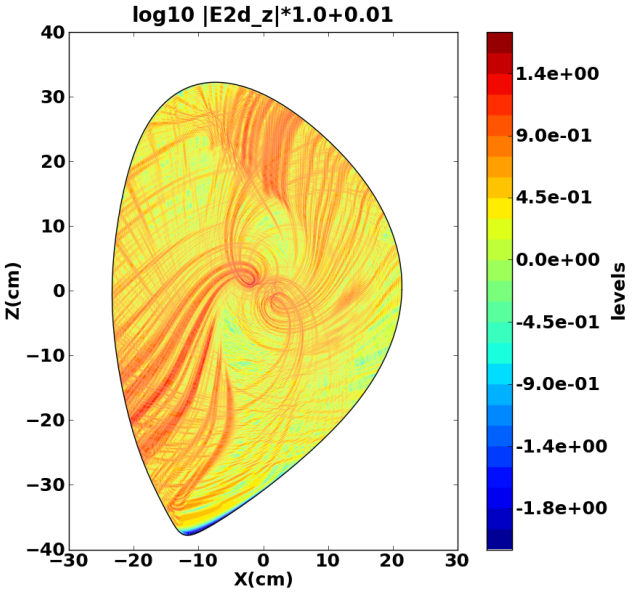

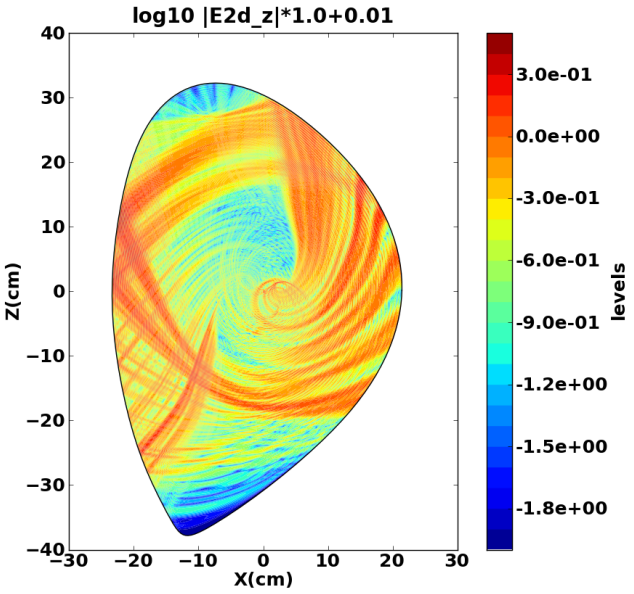

- Upper left initial
- Lower left converged
- Upper right converged spectrum
- Lower right converged power

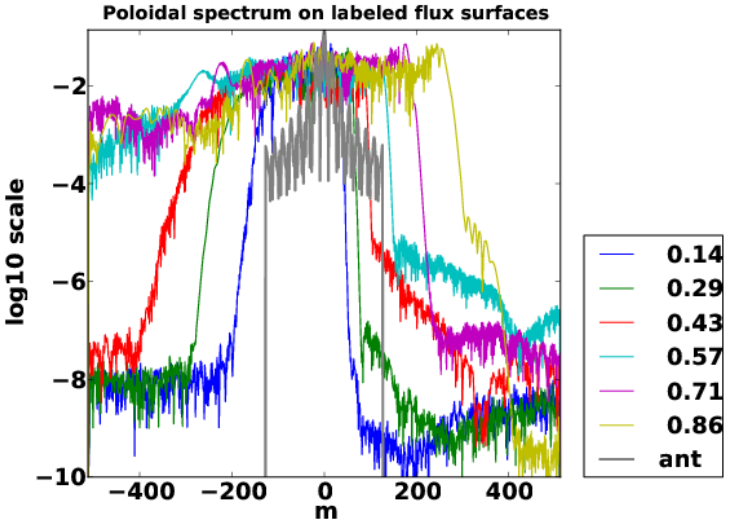

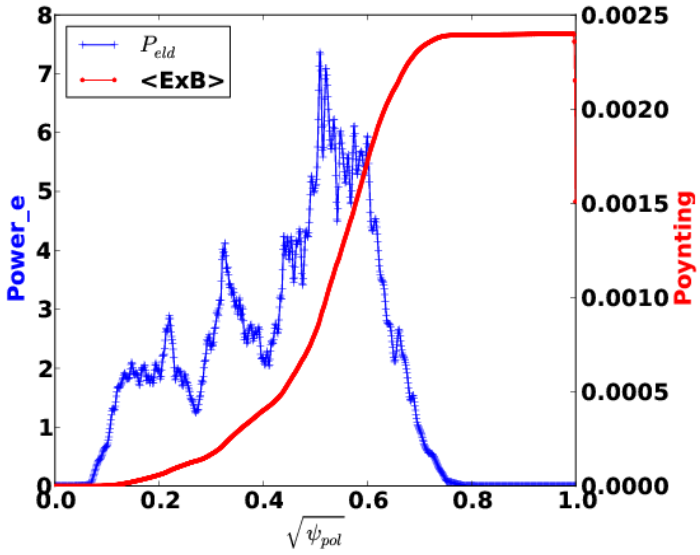

C-Mod $n_{\|} = -3.1$

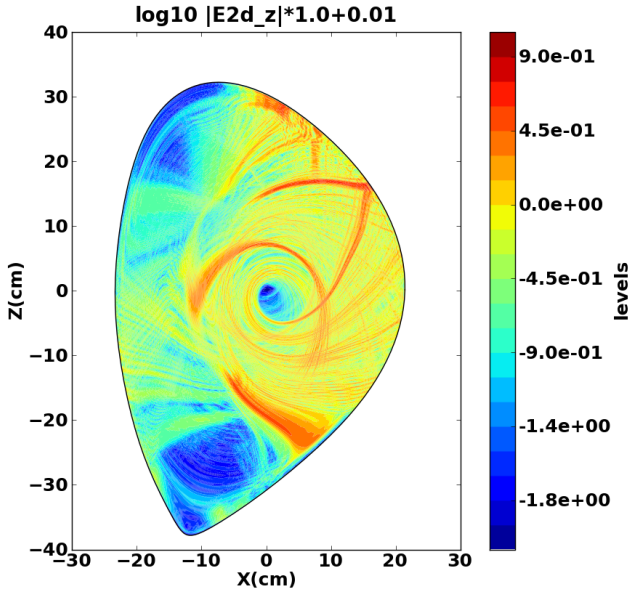

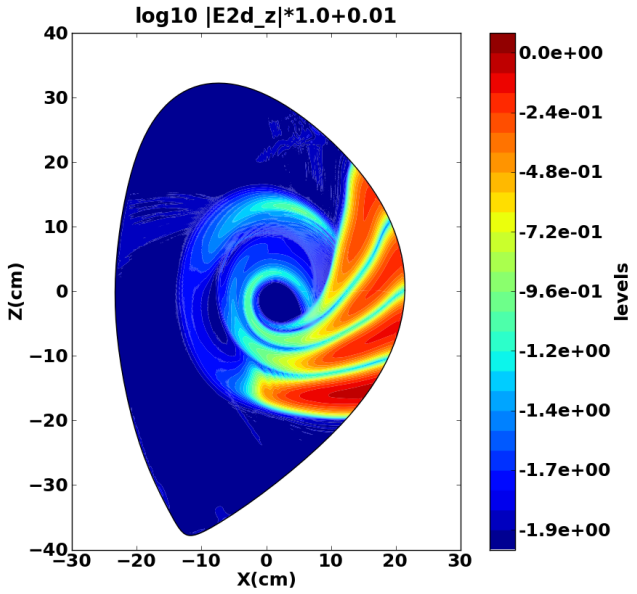

- Upper left initial
- Lower left converged
- Upper right converged spectrum
- Lower right converged power

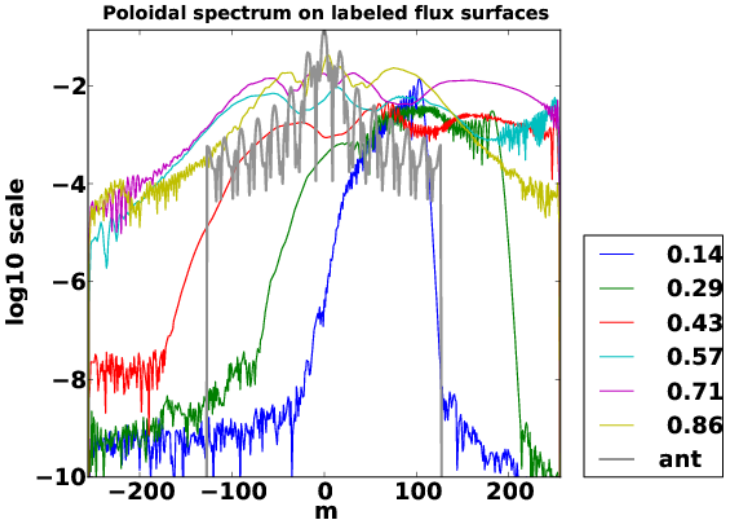

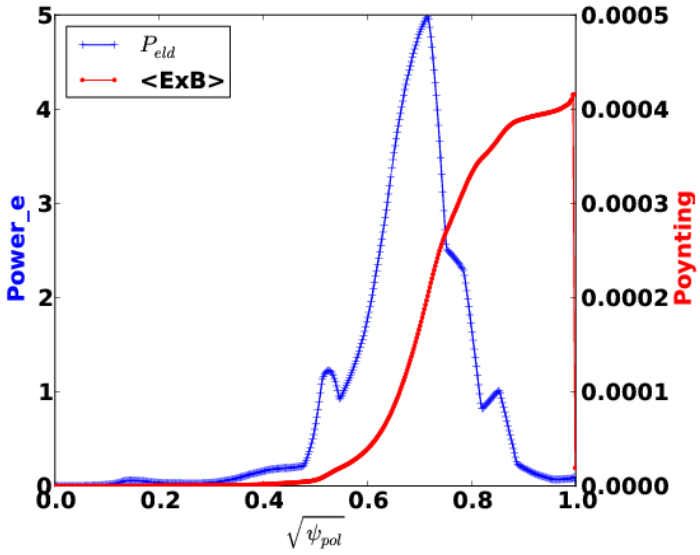

/home/jwright/TORIC_RUNS/618/Step13/TORICLH.cdf

Strong damping in Alcator C-Mod using 13 automated iterations

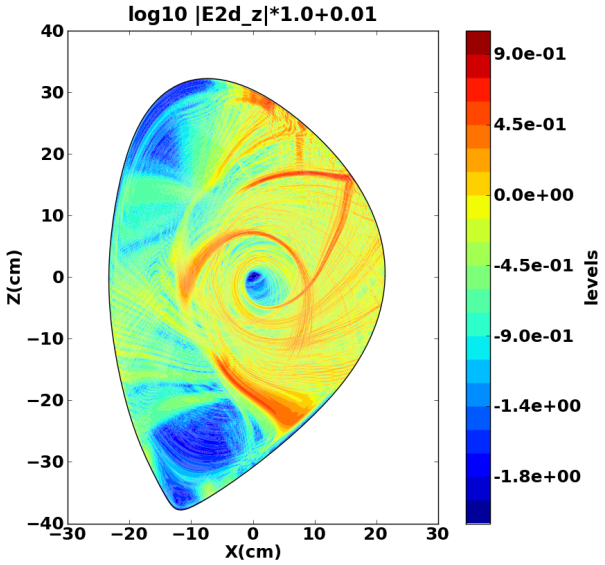

← Initial state

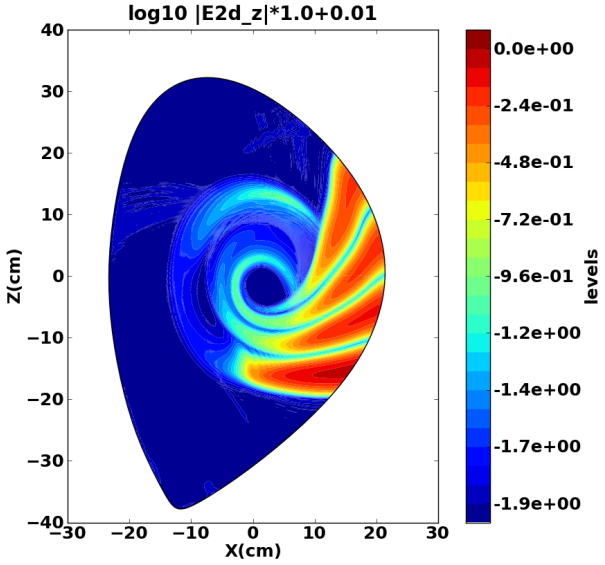

← Final state

Results:

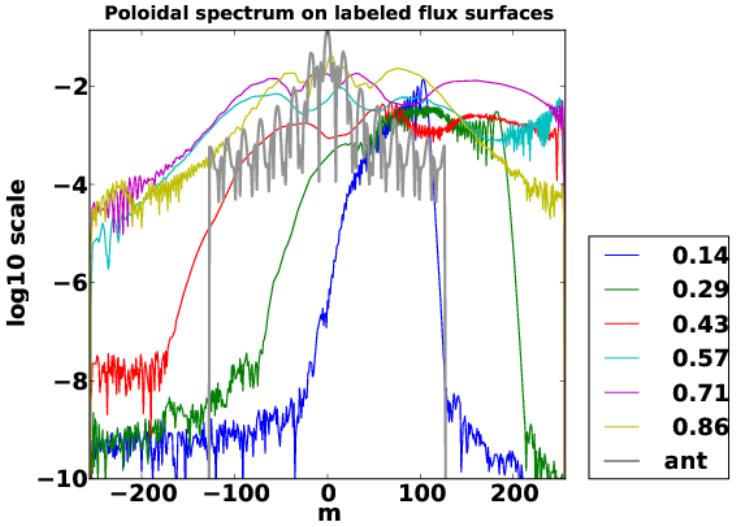

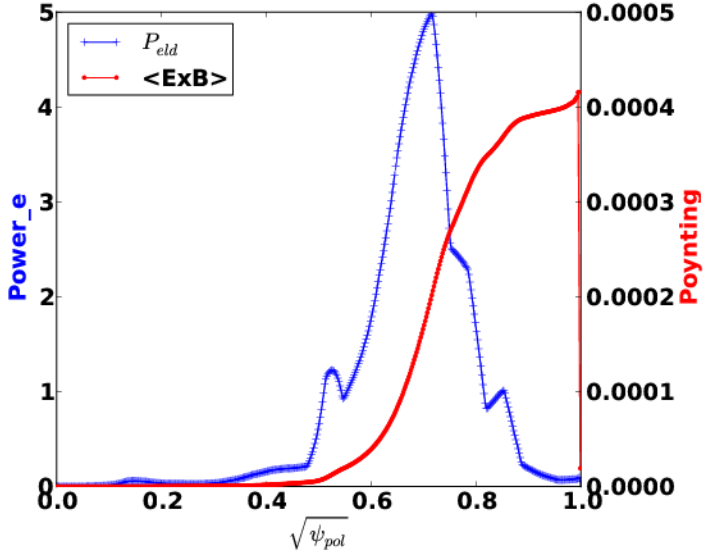

Strong damping iteration more easily converged.

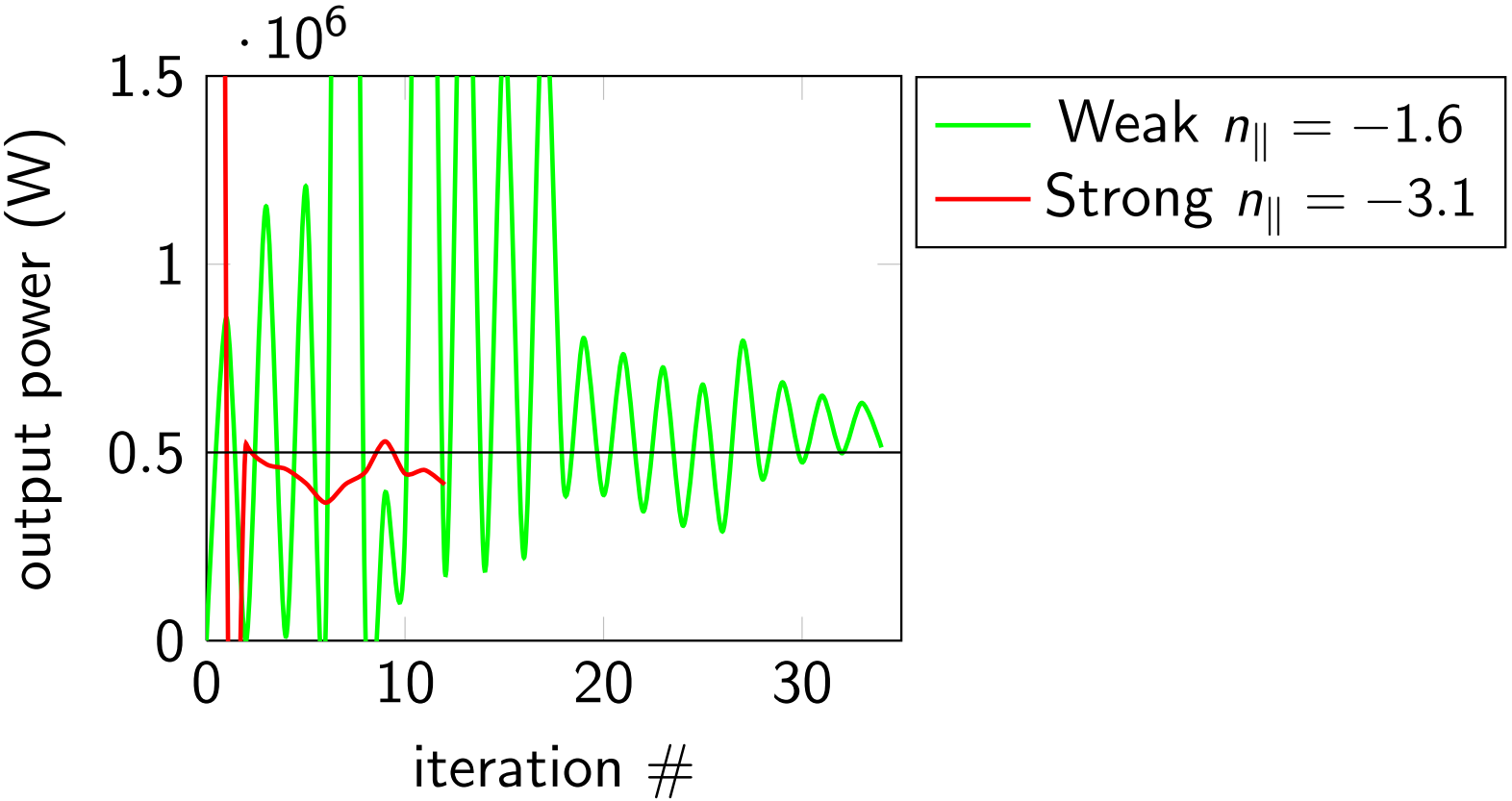

- Target power of 500kW for Alcator C-Mod
- Large oscillations in weak absorption case which eventually settle.

Too slow: More numerical techniques

Vector Acceleration methods for iteration

- MPE and RRE techniques improve rate of convergence of fixed point iteration methods. Similar to Krylov subspace methods (eg GMRES) [Sidi, 2008].

$$\begin{aligned} \Psi(x = s) &= 0 \\ x_{n+1} &= F(x_n) \\ \text{linearize about fixed point,} s: &= F(s) + F'(s)(x_n - s) \\ x_{n+1} &= F'(s)x_n + (1 - F'(s))s = Tx_n + b \end{aligned}$$

- This is a linear system of size N. Apply acceleration to inverse.
- Sample the system with $k << N$ iterations.
- Construct inverse through least squares constraint minimizing error $(x_{n+1} - x_n)$ to optimally project to solution.
- Solution is a linear superposition of iterations, $s = \sum_{i=1}^{k} c_i x_i$.

Acceleration of LH iteration reduces error in steady state.

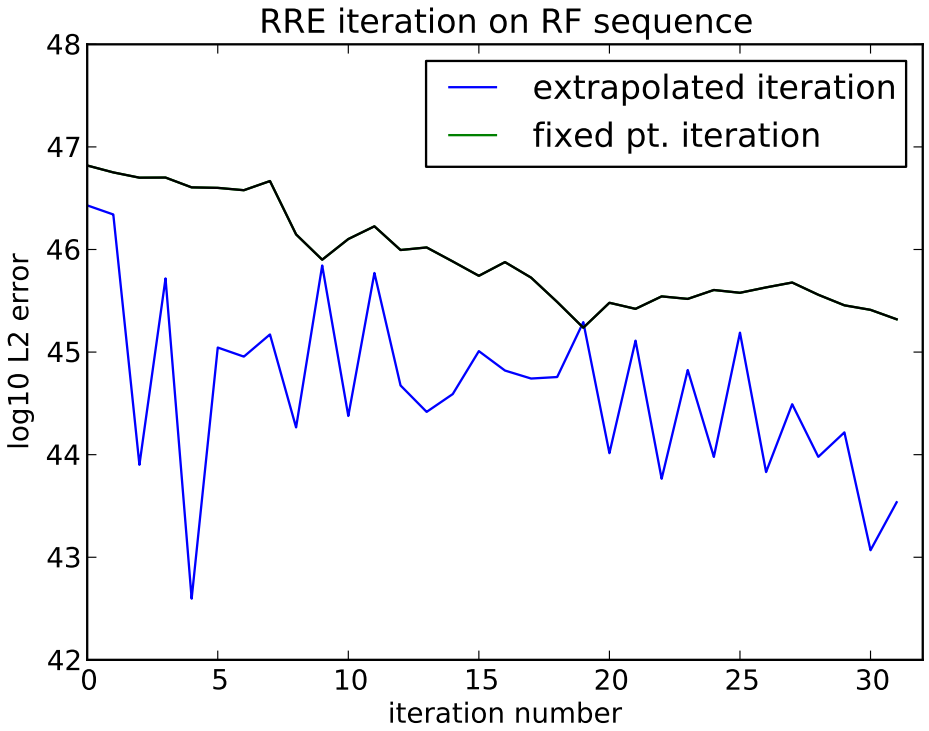

- $\log_{10}$ of L2 norm of error shown. Power is now accurate to within 1%.
- Refinement of solution takes less than 10 minutes with gain in accuracy of $\gg 10$ times.
- Can do better with by restarting every 7-10 iterations: 'cyclic' MPE

Back to ICRF

Three polarizations are well separated in space and scale.

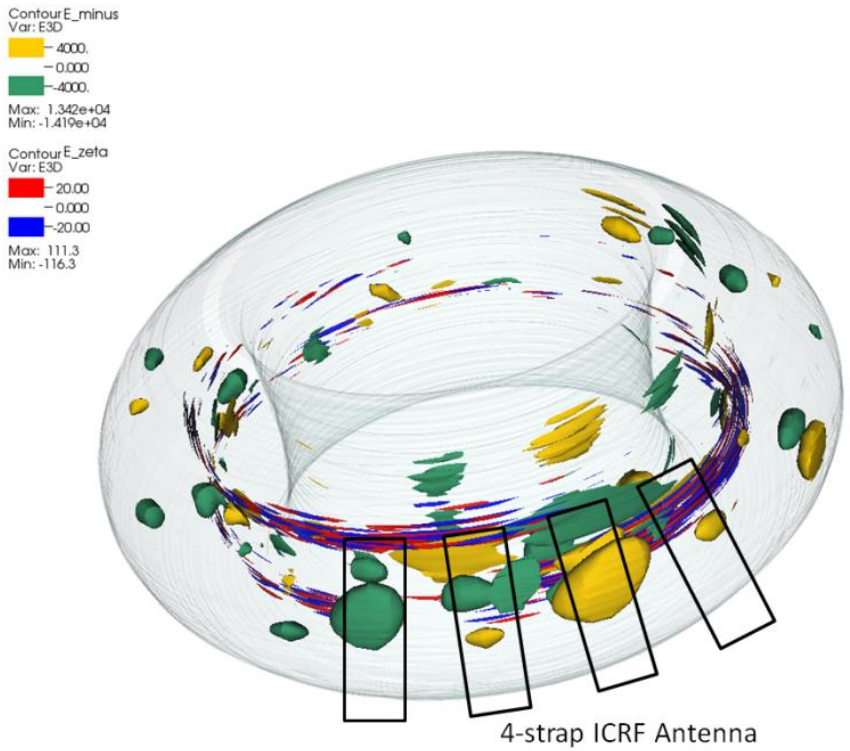

- In 3D we can see the direction of propagation, particularly of the ICW. The IBW is not distinguished in this view.
- 3D simulations are important for synthetic Phase Contrast Imaging (PCI) diagnostic.

Ion Cyclotron Absorption with Nonthermal Ion Tail Production

If "minority" ions species (eg 5% H) is present in a "majority" ion species plasma (95% D) then an RF wave with $\omega = \Omega_H$ will have an electric field component with the same polarization as the minority ion:

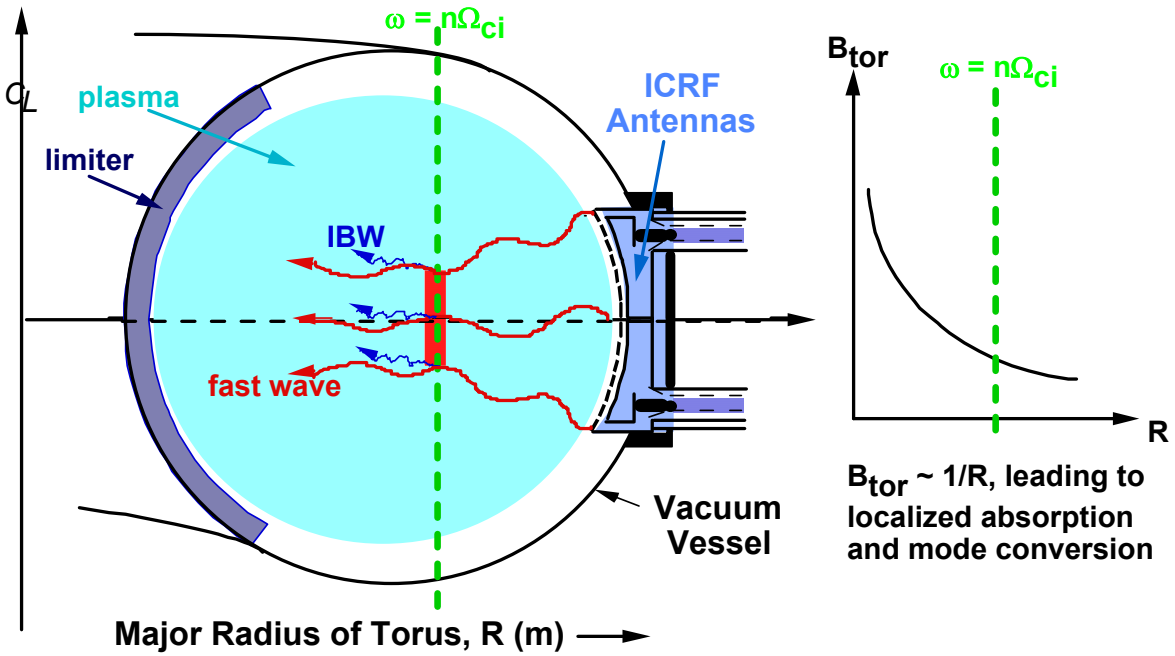

- Secular interaction - wave damps its power via cyclotron absorption on the minority ion.
- Nonthermal, anisotropic minority ion tail is generated that slows down and heats background electrons (drag) and majority ions (collisions).

Minority heating example shows intense fields at resonance [AORSA sim].

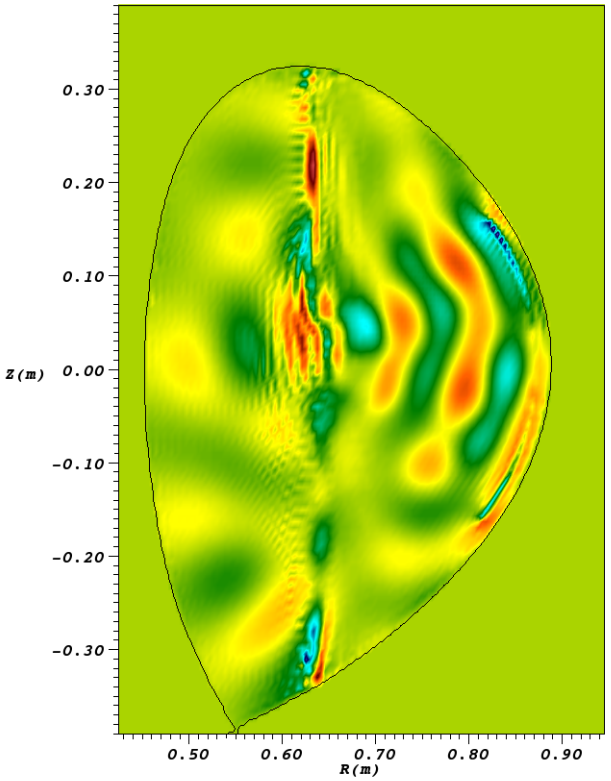

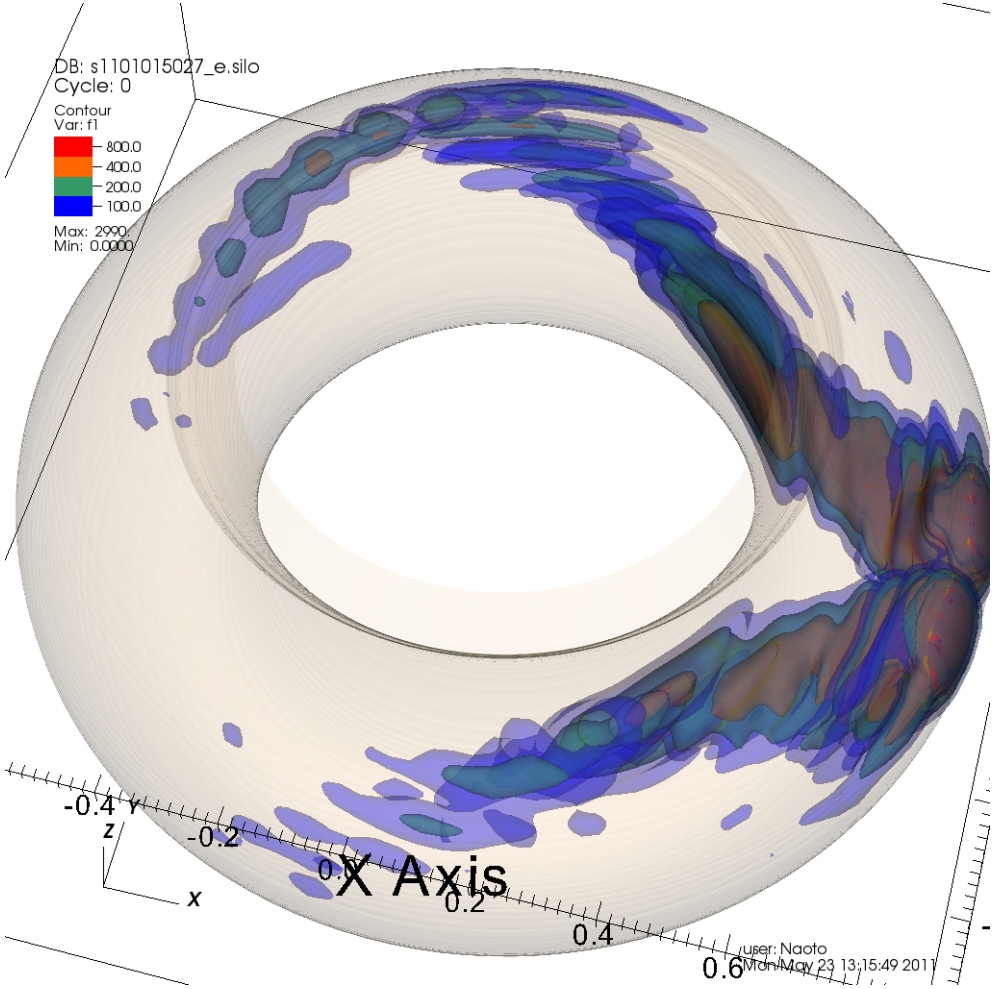

- Wavelengths on the order of several cm.
- Multipass nature of minority heating apparent in the 3-D rendering.
- 3-D fields obtained by superposing results from 40 toroidal modes.

Vector acceleration for implicit time advance of ICRF.

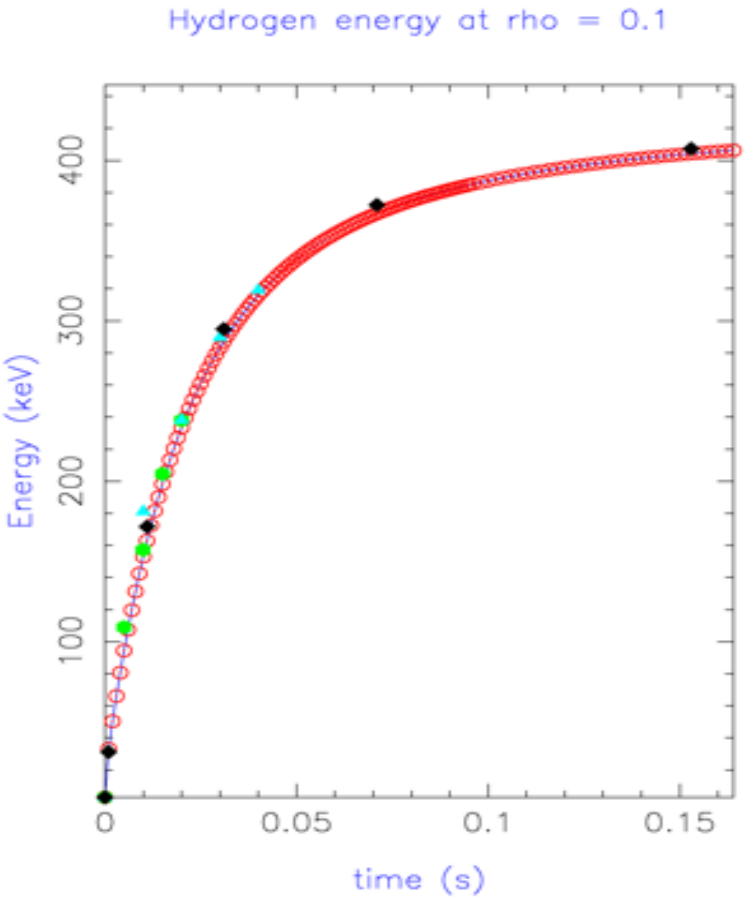

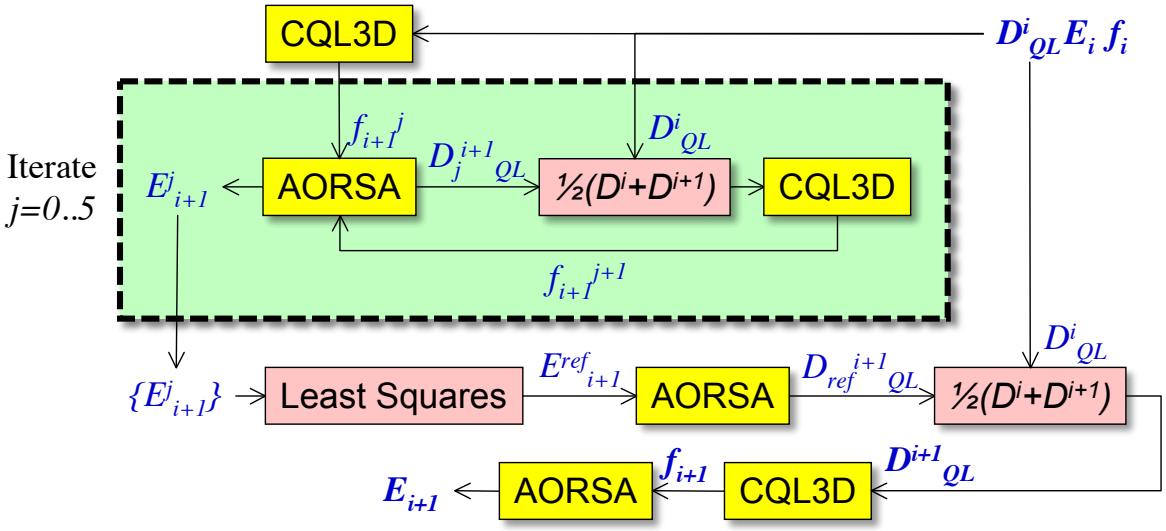

- Flow chart above showing the implicit advance of the distribution function and electric fields using a time centered RF diffusion operator.

- Implicit advance 3× faster than explicit. (2981 cpu-hrs vs 10368 cpu-hrs)

In collaboration with CSWIM SciDAC.

Validation

Phase Contrast Imaging (PCI) diagnostic measures ICRF waves 'directly'

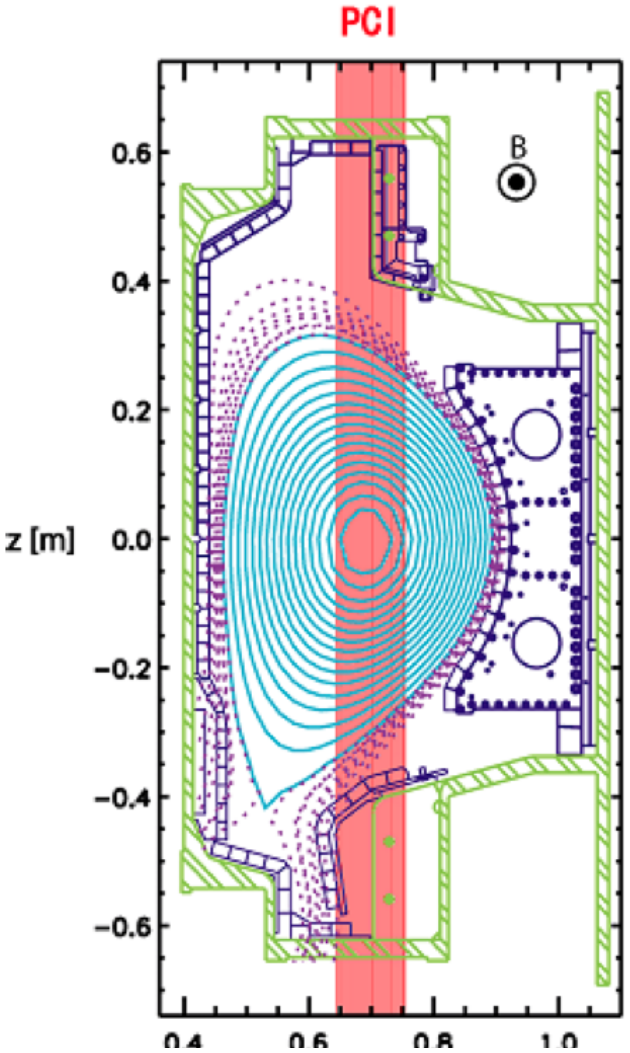

- PCI measures phase fluctuations in RF electric field and relates those to density fluctuations by scattering.

$$I_{\mathrm{PCI}} \propto \|E_0\|^2(1+2\tilde{\phi}) \sim \int dz \tilde{n}_e$$

- Density fluctuations in synthetic PCI are related to electric field through the electron momentum equation. More sophisticated model using consistent kinetic conductivity have been also implemented: [cite Nstujii]

$$n_e = \frac{i}{e\omega}\nabla\cdot(\sigma_e\cdot E)$$

Synthetic PCI comparison with experiment

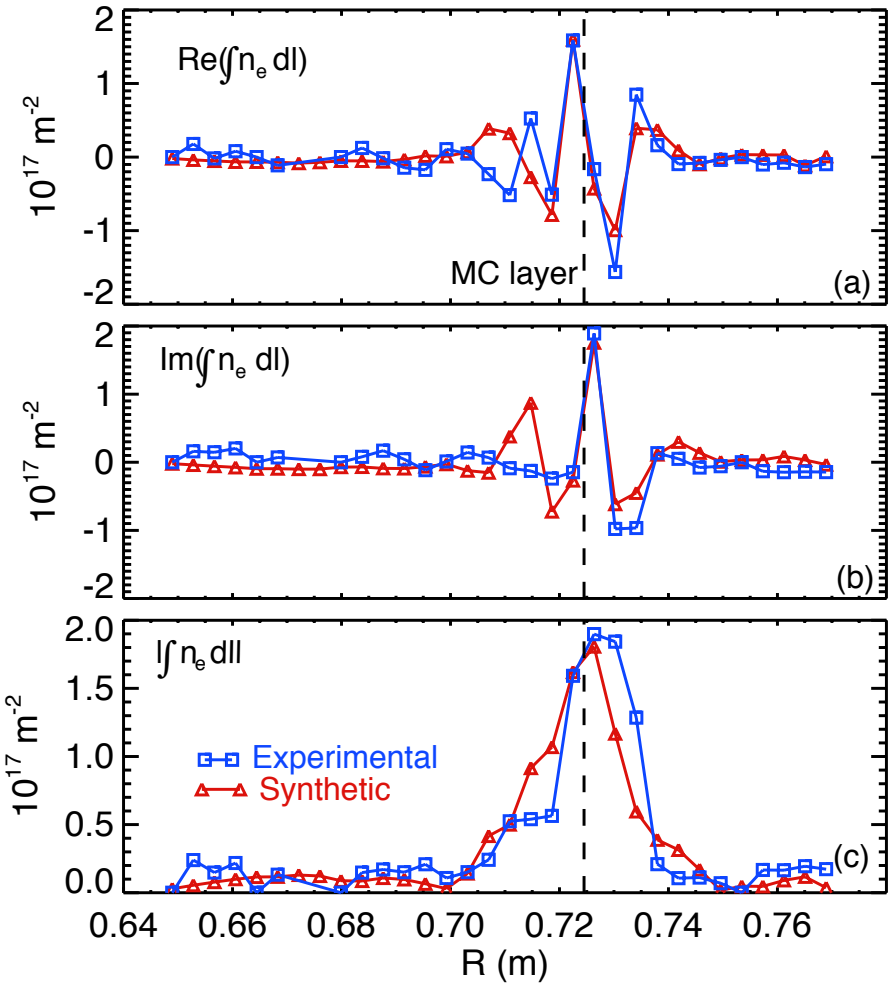

- Phase contrast imaging diagnostic is used to look at density fluctuations from ICRF waves on C-Mod
- Cases a) and b) show the real and imaginary part, c) the magnitude.
- Synthetic diagnostic identified aliasing in earlier verison of PCI with fewer channels [Lin *et al.*, 2004]
- Good agreement in some cases but not others. Possible edge effects, 3D uncertainty from antenna phase, uncertainty in minority concentration.

Compact Neutral Particle Analyzer (CNPA) for ICRF validation

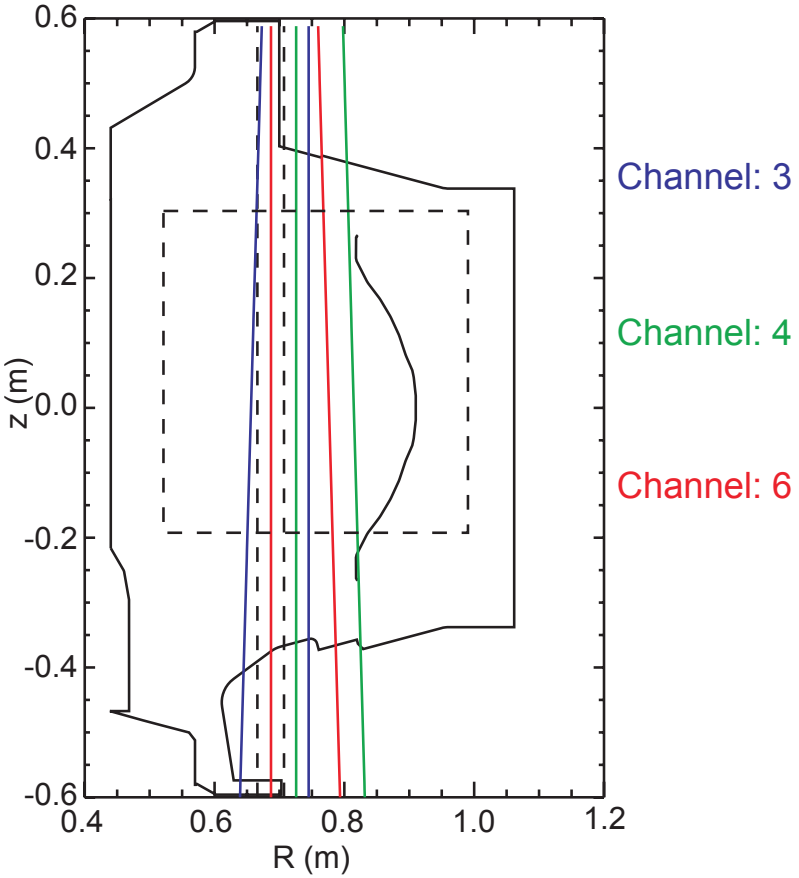

CNPA measures photons produced by charge exchange between energetic minority ions and background B or D along several vertical sightlines.

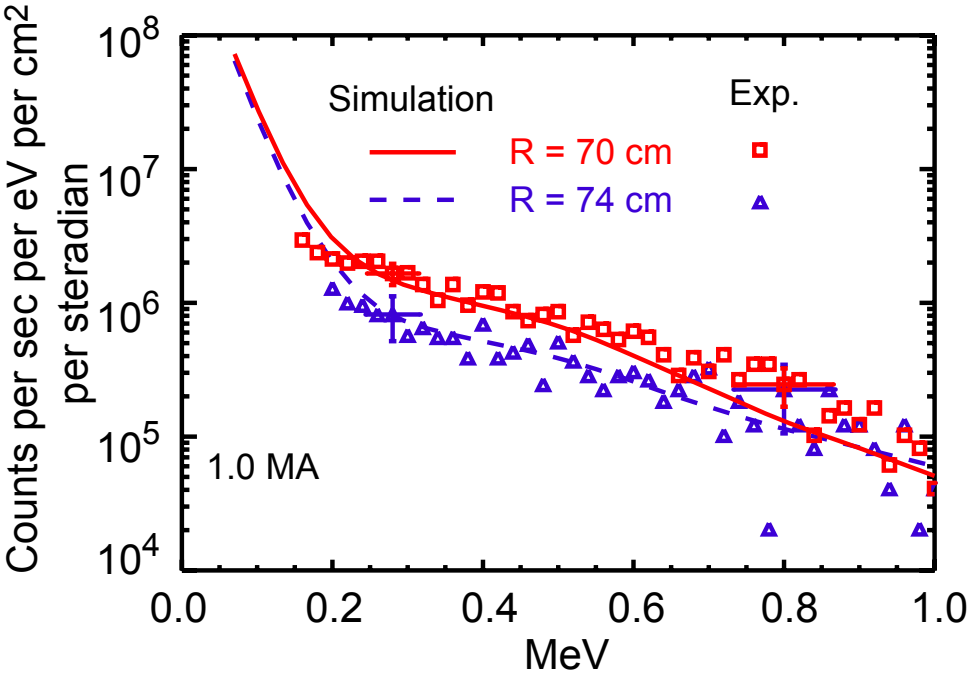

- Steady state comparison shows excellent agreement in magnitude and energy dependence.
- Further investigate shows that agreement during time evolution is not as good.

CNPA discrepancies appear in time dependence.

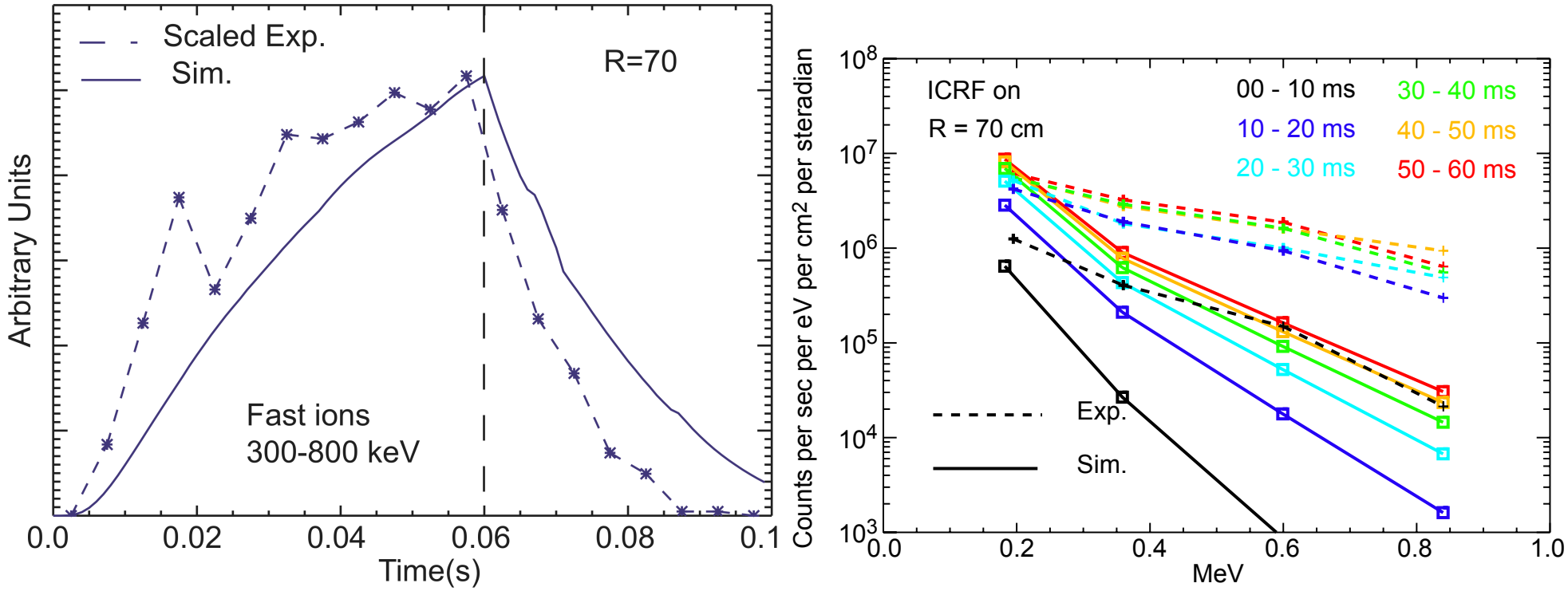

- The fast-ion distribution is seen to evolve faster in the experiment than it does in the simulation.
- Even larger discrepancies seen in energy spectrum.
- Dql model assumes decorrelation between interactions and that interactions are "small". But fast, 13 cpu-hrs = 1296 cpu x 0.614 min

DC for modeling particle response to RF

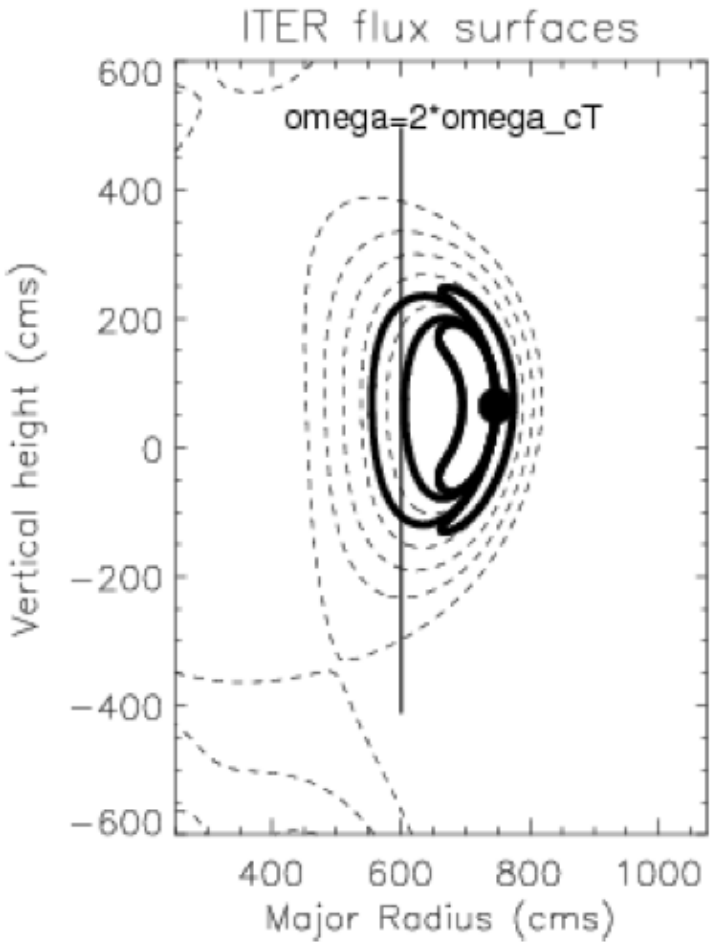

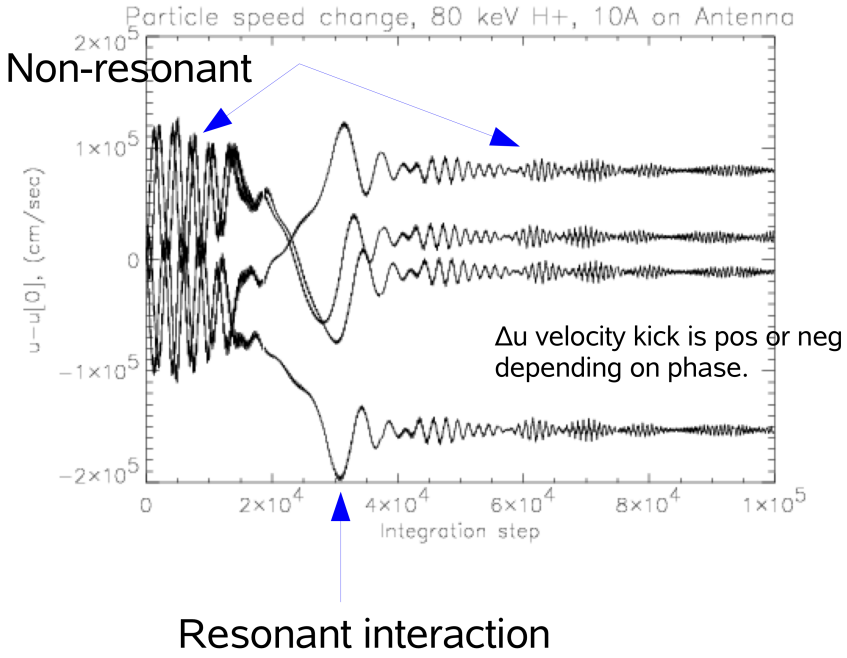

- The diffusion coefficent (DC) code calculates $D = \langle \delta v \delta v \rangle / \delta t$ from Newtonian orbits in the RF fields.
- Averages are done over cyclic directions (gyro motion and toroidal angle)

Correlation effects increase calculated perpendicular energy.

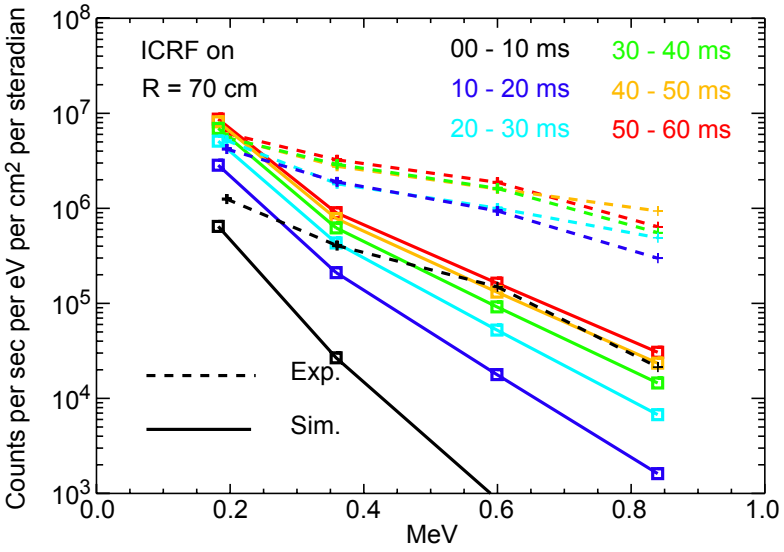

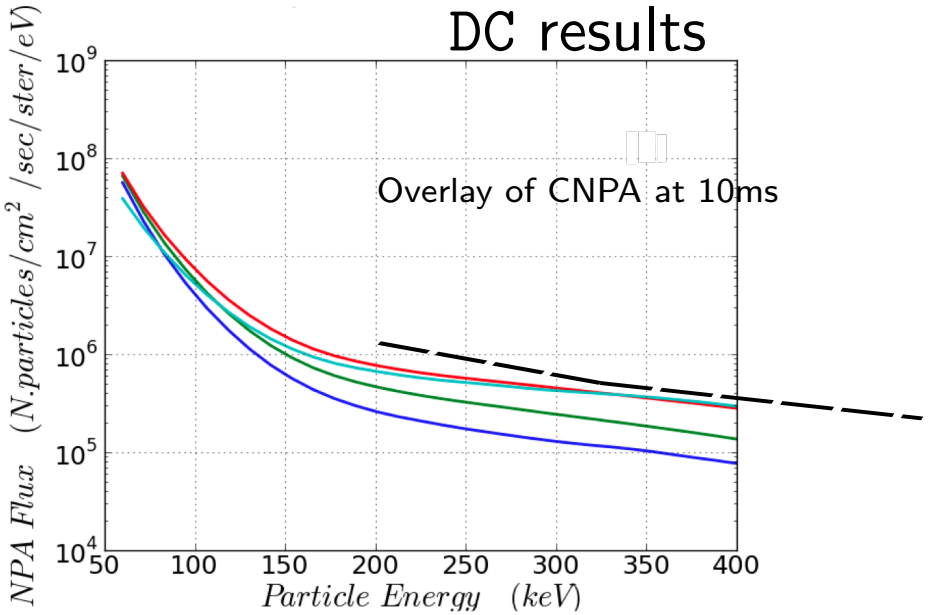

- Accounting for correlations and "large" non-diffusive kicks significantly increases agreement.
- Indicates importance of including more complete physics for these energetic ions.
- Comes at a cost: 28672 cpu-hrs vs 13 cpu-hrs

HXR diagnostic on Alcator C-Mod

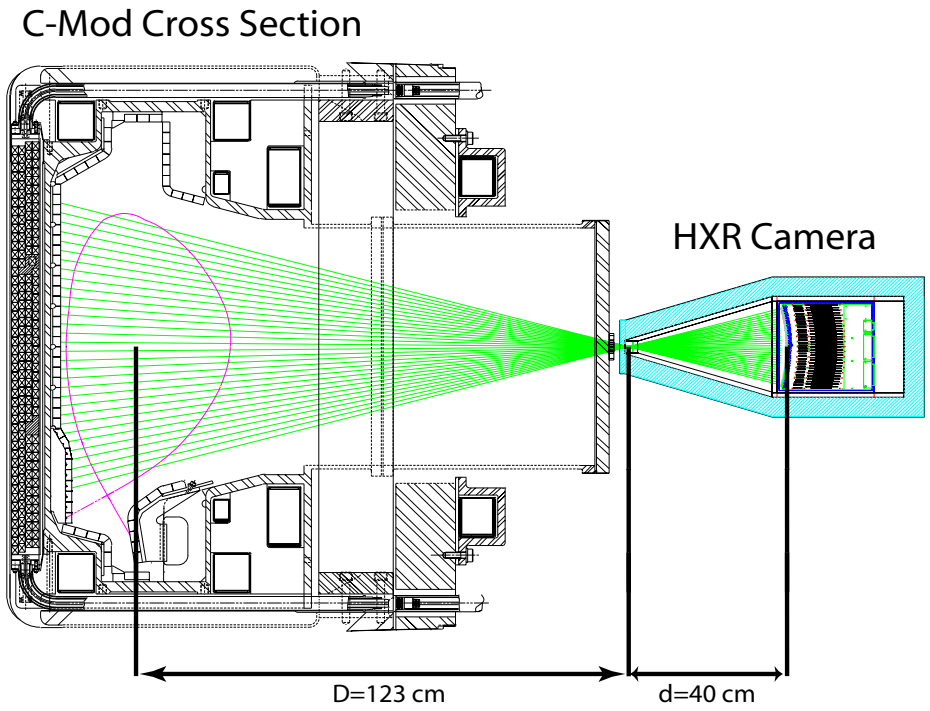

Figure Courtesy John Liptac

- 32 chords, measures X-rays from LH accelerated electrons that have been pitch angle scattered
- A synthetic hard X-ray diagnostic in `CQL3D` uses the same geometry to produce a signal for comparison.

HXR comparison using synthetic HXR

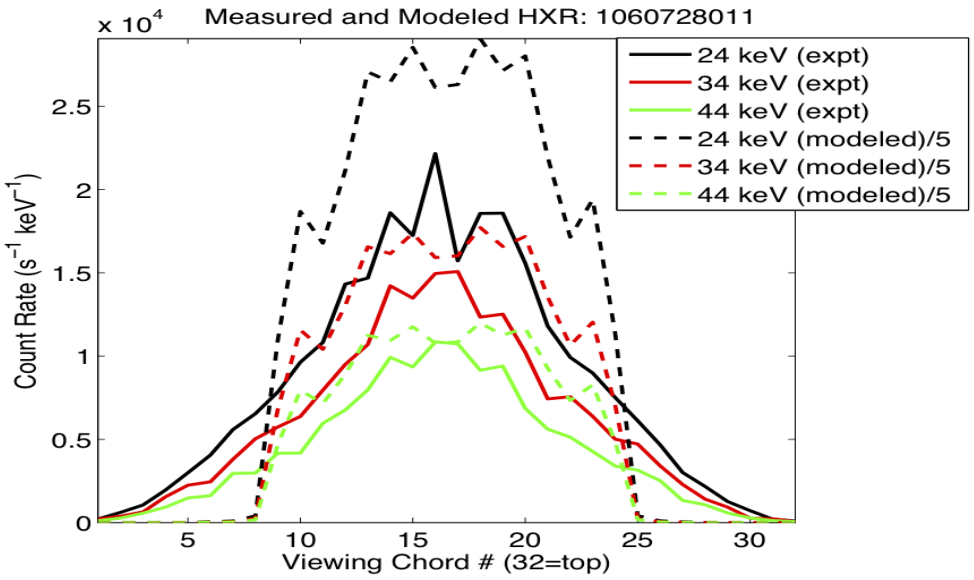

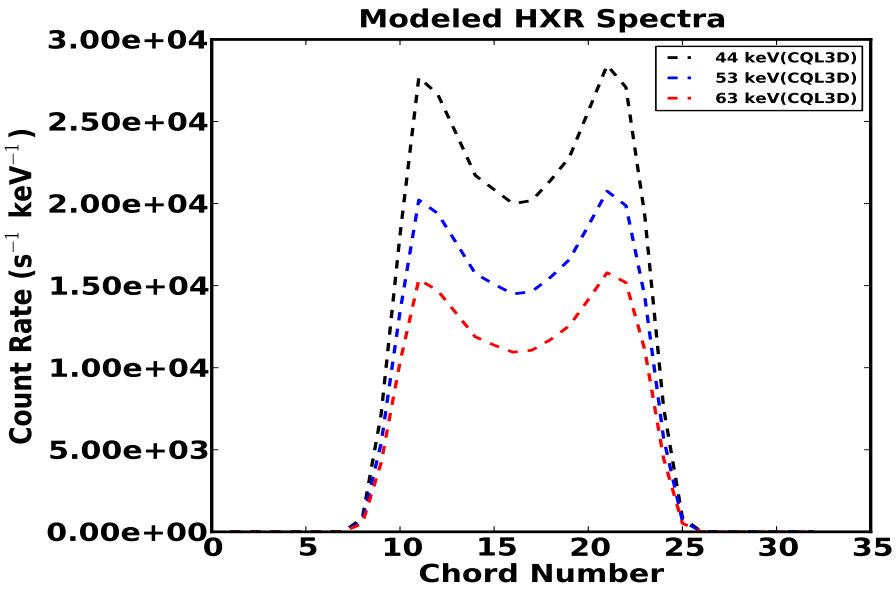

[Schmidt Diss. 2011]

- Comparison of measured and modeled HXR profiles for shot 1060728011 with $n_{\|} = -1.55$.
- Modeled profiles from ray tracing (left panel) have been scaled by a factor of 1/5 and those from full wave (right panel) have not been scaled. May be linked to interference effects in Dql from full wave.
- Both and are narrower in spatial extent than experiment.

Future directions

- GPUs/many-core CPUs and the general trend of data locality: flops are free.
- Non spectral wave solvers + particle based dielectrics
  Going to the edge.
- Time domain and non-linear effects: RF sheaths, parametric instabilities

Conclusions

- A good algorithm beats a faster computer any day of the week.
- Faster computers do help though: enabling higher fidelity models
- Combined, new ways of exporing physics : higher dimensionality, more resolution, ensemble studies, integrated modeling

References and further reading

Garaud, P. and Garaud, J. D. (2008).

Dynamics of the solar tachocline II. The stratified case. *Mon. Not. R. Astron. Soc.* **391**, 1239–1258.

Harvey, R. W. and McCoy, M. G. (1993).

The CQL3D Fokker-Planck Code. In *Proc. of the IAEA Tech. Committee Meeting (Montreal,1992)*, pages 489–526, Vienna. IAEA, Institute of Physics Publishing; USDOC/NTIS Doc. DE93002962.

Jaeger, E. F., Berry, L. A., D´Azevedo, E., Batchelor, D. B., Carter, M. D., and White, K. F. (2002).

Advances in full-wave modeling of radio frequency heated, multidimensional plasmas. *Phys. Plasmas* **9**, 1873–1881.

Jaeger, E. F., Berry, L. A., Myra, J. R., Batchelor, D. B., D´Azevedo, E., Bonoli, P. T., Phillips, C. K., Smithe, D. N., DÍppolito, D. A., Carter, M. D., Dumont, R. J., Wright, J. C., and Harvey, R. W. (2003).
Sheared Poloidal Flow Driven by Mode Conversion in Tokamak Plasmas. *Phys. Rev. Lett.* **90**, 195001.

Lee, J.-P. and Wright, J. C. (2013).

A versatile parallel block tri-diagonal solver for spectral codes. *Commun. Comput. Phys.* -, –. under review.

Lin, Y., et al (2004).

Investigation of ion cyclotron range of frequencies mode conversion at the ion–ion hybrid layer in Alcator C-Mod. *Physics of Plasmas* **11**, 2466–2472.

Nelson-Melby, E., Porkolab, M., Bonoli, P. T., Lin, Y., Mazurenko, A., and Wukitch, S. J. (2003).

Experimental Observations of Mode-Converted Ion Cyclotron Waves in a Tokamak Plasma by Phase Contrast Imaging. *Phys. Rev. Lett.* **90**, 155004.

Perkins, F. W. (1977). Heating Tokamaks via the Ion-Cyclotron and Ion-Ion Hybrid Resonances. *Nucl. Fusion* **17**, 1197.

Sidi, A. (2008).

Vector extrapolation methods with applications to solution of large systems of equations and to PageRank computations. *Comput. Math. Appl.* **56**, 1–24.

Stix, T. H. (1992). *Waves in Plasmas*, chapter 10, page 250. American Institute of Physics, New York.

Wright, J. C., Lee, J., et al Challenges in Self-Consistent Full-Wave Simulations of Lower Hybrid Waves.

IEEE Transactions on Plasma Science **38**, 2136–2143.